Available online at www.sciencedirect.com

ScienceDirect

Russian Geology and Geophysics 58 (2017) 1263–1269

RUSSIAN GEOLOGY AND GEOPHYSICS

www.elsevier.com/locate/rgg

Subsurface geoelectric array with two transmitters for petroleum exploration in offshore areas

A.V. Marinenko [a,*], M.I. Epov [a,b]

[a] *A.A. Trofimuk Institute of Petroleum Geology and Geophysics, Siberian Branch of the Russian Academy of Sciences, pr. Akademika Koptyuga 3, Novosibirsk, 630090, Russia*

[b] *Novosibirsk State University, ul. Pirogova 2, Novosibirsk, 630090, Russia*

Received 16 August 2016; accepted 6 December 2016

Abstract

At present, sounding methods based on the effect of electromagnetic pulses on the environment are widely used for marine exploration of hydrocarbon deposits. The exploration is performed using research systems with special equipment fixed in the water column. The goal of this work is to develop equipment and methods for marine electrical prospecting that would allow reliable predictions of petroleum fields in the underlying environment with reduced labor intensity of the necessary surveys. For this purpose, a subsurface array for marine electrical prospecting during vessel movement is proposed. The effective frequencies, current strengths in cables, and the size and efficiency of the array are determined using both the theoretical knowledge of the operation of similar arrays in similar environments and numerical simulation of the developed array. The 3D finite element method is used for mathematical modeling.

Keywords: marine geophysics; electric array; finite element method; electric field; electrical conductivity; electric charge

Introduction and problem statement

The main problem of marine geoelectrical exploration is the screening effect of the highly conducting seawater layer. The easiest way to eliminate this effect is to place the entire array or its parts (measuring probes) near the seabed (Davydycheva and Rykhlinski, 2011). This approach is obvious, but the corresponding technologies require very complex and costly technical solutions. Because of the strong influence of the conductive seawater layer on the measured signals, the arrays commonly used in surface electrical exploration are brought nearer to target objects by placing them at the bottom or at a small distance from it. This is of course a forced decision, which leads to major difficulties in practice, such as transportation of the array along the uneven seabed, its inaccurate positioning, etc. The use of subsurface arrays is possible if they have low sensitivity to the seawater layer and if the measured signal provides a sufficient amount of information to identify petroleum deposits and determine their structure, distribution, and specific electrical conductivity (SEC).

A similar problem, associated with the wide use of highly conductive biopolymer salt-based drilling muds, was encountered in borehole geophysics (Epov and Antonov, 2000). The logging unit (probe) is in a penetrating borehole filled with a highly conductive homogeneous drilling mud. For such models, approximate expressions describing the electromotive force (EMF) of a current turn of short radius (but comparable to the length of the probe) were obtained as early as in the 1970s. It was assumed that the borehole is in a homogeneous conductive medium.

$$\xi^{(2)}(k_1 r_1, k_2 L) \approx \frac{\xi^{(1)}(k_2 L)}{I_0^2(k_1 r_1)}. \quad (1)$$

Here $\xi^{(2)}$ is the EMF in the two-layer nonmagnetic medium [V]; $\xi^{(1)}$ is the EMF in the homogeneous nonmagnetic external environment [V]; r_1 is the radius of the borehole [m]; k_1 and k_2 are the wavenumbers in the external and borehole environments; I_0 is a modified Bessel function of zero order. In the quasi-stationary approximation, we assume that the influence of the bias currents is small:

$$k_j^2 = -i\omega\mu_0\sigma_j, \quad j = 1, 2,$$

* Corresponding author.
E-mail address: arkadiy@reqip.net (A.V. Marinenko)

1068-7971/$ - see front matter © 2017, V.S. Sobolev IGM, Siberian Branch of the RAS. Published by Elsevier B.V. All rights reserved.
http://dx.doi.org/10.1016/j.rgg.2016.12.011

where σ_1 is the SEC of the drilling fluid; σ_2 is the SEC of the external environment; $\mu_0 = 4\pi \times 10^{-7}$ H/m is the magnetic permeability of vacuum; ω is the cyclic frequency [s^{-1}]; L is the distance between the transmitter and the measured point (probe length) [m]. Comparative analysis of calculations using accurate expressions and approximate formulas has shown that relation (1) is sufficiently accurate for practice if $\left|k_1 L\right|$, $\left|k_2 L\right| > 1$. Furthermore, the accuracy increases if $\sigma_1 > \sigma_2$.

The second condition necessary for the signal to be well approximated by relation (1) is $\frac{L}{r_1} \geq 5$, i.e., the length of the probe should be several times the radius of the borehole.

Note an important feature of relation (1): on the logarithmic scale, the EMF in the two-layer medium is the sum of two contributions—from the borehole and the external environment:

$$\ln \overline{\xi}^{(2)}(k_1 r_1, k_2 L) = \ln \overline{\xi}^{(1)}(k_2 L) + \ln I_0^2(k_1 r_1), \tag{2}$$

where $\xi^{(1)}$ and $\xi^{(2)}$ are the nondimensionalized EMFs.

In relation (2), the second term depends only on the parameters of the borehole and is independent of the separation L. We consider the expression for the EMF at two separations, L_1 and L_2:

$$\ln \left|\overline{\xi}^{(2)}(k_1 r_1, k_2 L_1)\right| = \ln \left|\overline{\xi}^{(1)}(k_2 L_1)\right| + \ln I_0^2(k_1 r_1),$$

$$\ln \left|\overline{\xi}^{(2)}(k_1 r_1, k_2 L_2)\right| = \ln \left|\overline{\xi}^{(1)}(k_2 L_2)\right| + \ln I_0^2(k_1 r_1).$$

Subtracting one equality from the other, we obtain:

$$\ln \left|\overline{\xi}^{(2)}(k_1 r_1, k_2 L_1)\right| - \ln \left|\overline{\xi}^{(2)}(k_1 r_1, k_2 L_2)\right|$$

$$= \ln \left|\overline{\xi}^{(1)}(k_2 L_1)\right| - \ln \left|\overline{\xi}^{(1)}(k_2 L_2)\right|. \tag{3}$$

It is seen from relation (3) that the difference between the logarithms of the normalized EMFs in this approximation is independent of the borehole radius and the SEC of the drilling fluid.

The measured quantities can be represented in terms of the amplitudes $|\overline{\xi}|$ and the phases φ:

$$\overline{\xi} = |\overline{\xi}|\, e^{i\varphi}. \tag{4}$$

Then relation (3) can be rewritten as

$$\ln \left|\overline{\xi}^{(2)}(k_1 r_1, k_2 L_1)\right| - \ln \left|\overline{\xi}^{(2)}(k_1 r_1, k_2 L_2)\right|$$

$$= \ln \left|\overline{\xi}^{(1)}(k_2 L_1)\right| - \ln \left|\overline{\xi}^{(1)}(k_2 L_2)\right|,$$

$$\ln \left|\frac{\ln \overline{\xi}^{(2)}(k_1 r_1, k_2 L_2)}{\ln \overline{\xi}^{(2)}(k_1 r_1, k_2 L_1)}\right| = \ln \left|\frac{\overline{\xi}^{(1)}(k_2 L_2)}{\overline{\xi}^{(1)}(k_2 L_1)}\right|, \tag{5}$$

$$\varphi^{(2)}(k_1 r_1, k_2 L_2) - \varphi^{(2)}(k_1 r_1, k_2 L_1) = \varphi^{(1)}(k_2 L_2) - \varphi^{(1)}(k_2 L_1). \tag{6}$$

Thus, in this approximation, the ratios of the EMF amplitudes and the phase differences measured at two distances from the transmitter depend only on the parameters of the homogeneous external environment.

Methodology of the study

Now let us return to the problem of marine geoelectrical exploration. We consider a three-layer geoelectrical model with two plane-parallel boundaries. The top layer is nonconducting, the middle layer is highly conductive seawater, and the bottom layer is the underlying conductive space (earth). We introduce a Cartesian system of coordinates in which the plane $x0y$ coincides with the boundary between the first and second layer, and the z axis is directed perpendicularly downward (Fig. 1). The position of the boundary between the first and second layer is described by the equation $\overline{Z} = 0$, and that between the second and third layer, by the equation $\overline{Z} = h$. The top and bottom boundaries will be considered so remote that they virtually do not affect the calculated fields.

Using the analogy with the logging problem and the method of obtaining the approximate expression (1), we can write the following expression for the EMF ξ on the surface of the laterally homogeneous seawater layer underlain by the conducting half-space:

$$\xi(k_1, k_2, h, L) \approx \xi(k_2, L) \cdot e^{-2k_1 h}, \tag{7}$$

where k_1 and k_2 are the wavenumbers, h is the thickness of the seawater layer, L is the distance between the transmitter and receiver (separation).

Taking the natural logarithm of expression (7) and using the nondimensionalized EMFs, we obtain:

$$\ln\left(\overline{\xi}(k_1, k_2, r, L)\right) \approx \ln\left(\overline{\xi}(k_2, L)\right) - 2k_1 h. \tag{8}$$

Thus, the influence of the seawater layer can be weakened by calculating the following quantity:

$$\ln\left(\xi(k_1, k_2, h, L_1)\right) - \ln\left(\xi(k_1, k_2, h, L_2)\right)$$

$$\approx \ln\left(\xi(k_2, L_1)\right) - \ln\left(\xi(k_2, L_2)\right). \tag{9}$$

As shown above, this quantity can be converted into the phase difference (6). By setting the separation in the array and calculating the phase difference between the measurement electrodes, it is possible to significantly reduce the effect of seawater layer.

However, this approach does not account for the unique property of the seawater layer that its physical properties such as salinity and temperature are inhomogeneous with depth (Luz and Regis, 2009). In measurements of seawater temperature at different depths, the water column is conditionally divided into three layers (Fig. 2, left): a surface layer, a layer with an abrupt temperature change (thermocline), and a deep-water layer. The temperature changes in the surface and deep-water layers are less significant than the temperature jumps in the thermocline. This is due to the fact that the upper layer of seawater is well mixed by the winds, and sunlight does not penetrate into the deep-water layer.

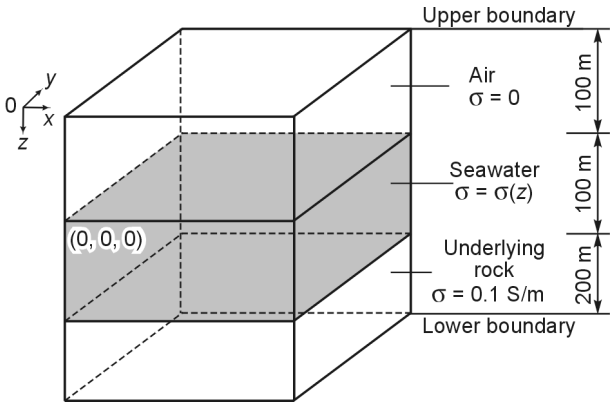

Fig. 1. Geoelectric model.

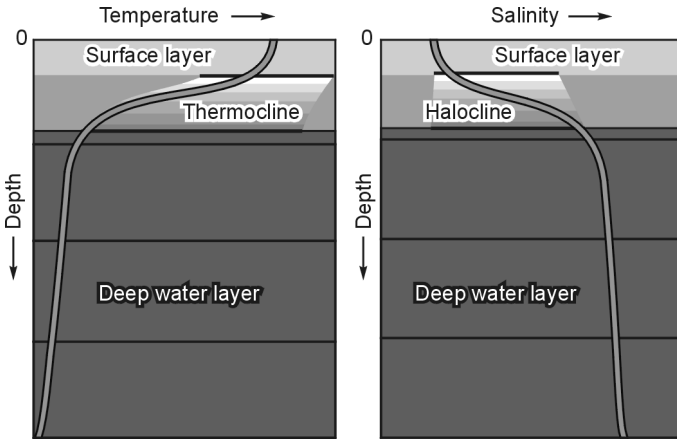

Fig. 2. Changes in water temperature and salinity with depth.

In salinity measurements at different depths, the water column is also divided into three layers (Fig. 2, right): a surface layer, a layer with an abrupt salinity change (halocline), and a deep-water layer. Furthermore, in different parts in the same sea, the thickness of these temperature and salinity zones may be different. Traditionally, the SEC of seawater at different depths is calculated from its temperature and salinity using special tables (Unesco, 1981). Actual experiments have shown that descriptions of temperature and salinity variations with depth using linear functions and generalized to great depth are often correct. However, when using transmitters with a nonzero vertical electric field component for electromagnetic sounding, a space charge is formed in seawater (Marinenko et al., 2009). In this case, if the SEC of seawater is defined as a constant, the results of numerical modeling may be not realistic (Marinenko et al., 2009). Thus, the change in the SEC of seawater with depth should be taken into account in modeling.

Selecting a sounding system

Let us make a brief comparative analysis of frequency-domain electromagnetic sounding systems. Electromagnetic field sources in marine electrical exploration are either closed loops with alternating current or segments of insulated electrical cables with current electrodes or toroidal coils on the ends. They can be either in a horizontal plane (parallel to the sea surface) or in a vertical plane (orthogonal to the sea surface). The transmitters are usually moving (move together with the vessel), and the receiver may be stationary or they can move together with the transmitters at a certain distance from them (Um and Alumbaugh, 2007). In galvanic sources (segments of electric cables), currents (1000 A and more) are passed through seawater using a simple electrode system (power consumption of about 100 kW (Constable and Srnka, 2007)). Transmitters of finite size are often replaced by point transmitters to obtain solutions in quadratures. It should be noted that the obtained solution of direct problems do not always satisfactorily describe real situations. The dipole approximation is considered valid if the distance to the receivers is large compared to the typical transmitter size (Landau and Lifshits, 2006). Streich and Becken (2011) have made an attempt to evaluate the modeling errors due to the replacement of a current cable by a horizontal electric dipole. An important issue in the comparative analysis of the systems is the external current waveforms—rectangular or sinusoidal. Connell and Key (2013) have made a numerical comparison of the influence of different shapes of external currents in shallow-water petroleum prospecting. When using rectangular pulses, maximum energy is transferred to the lower half-space as the current amplitude is maximal during the entire operation of the array (Rune and Tor, 2007). However, in practice, it is not technically possible to instantly switch the current from positive to negative. This requires finite time. This may lead to a model discrepancy between the measured signals and their synthetic analogs.

It is possible in principle to use a current loop as a transmitter. However, its use involves a number of technological difficulties. We will not consider the purely anomalous arrays where the transmitter and receiver are orthogonal to each other (Louise and Gerald, 1995). Despite the attractiveness of such configurations, it is almost impossible to ensure that they are orthogonal in actual soundings. Even a slight violation of this condition gives rise to electric field components closely related to the SEC and thickness of the seawater layer. In practice, the most widely used array consists of a floating insulated current cable and a set of measuring electrodes. Such a source generates both vertical and horizontal components of the electric current in the environment, in particular under the seabed. In this paper, we consider a modification of this source by adding a second insulated current cable perpendicular to the first. The dimensions, separations, and the ratio of the currents in its rays will be determined based on the suppression of part of the signal by the seawater layer.

An important characteristic of any array is the range of operating frequencies. Their values are conventionally determined by the condition that the skin layer thickness exceeds the thickness of the seawater layer. Based on this, the range

of operating frequency is from tenths of a hertz to hundreds of hertz. However, it should be borne in mind that the electric field is proportional to the frequency to a power not lower than the first, and decreasing the frequency reduces the signal and increases the noise/signal ratio (Keithley Instruments, 2013). Less stringent restrictions are imposed on the supply current value, which can vary from a few tens to several hundred amperes.

Mathematical model

After selecting the type of array, it is necessary to determine the mathematical tools used for the calculations. We use a three-dimensional vector finite element method in natural variables which allows obtaining all spatial components of the electromagnetic field and current density at the same points. The main features of the proposed algorithm are briefly described below.

Maxwell's equations describing electromagnetic processes are written in differential form as follows (Jackson, 1962):

$$\begin{cases} \operatorname{rot}\mathbf{E} = -\partial\mathbf{B}/\partial t; & \text{(Faraday's Law)} \\ \operatorname{rot}\mathbf{H} = \partial\mathbf{D}/\partial t + \mathbf{J} + \mathbf{j}^{e}; & \text{(Ampere's Law)} \end{cases} \tag{10}$$

$\operatorname{div}\mathbf{D} = \rho$ (Gauss's Law for electric induction),

$\operatorname{div}\mathbf{B} = 0$ (Gauss's Law for magnetic induction),

where $\mathbf{J}$ is the density of space currents (A/m^2); $\mathbf{j}^e$ is the external current density (A/m^2); ρ is the density of electric charges (C/m^3).

The electromagnetic-field components are four vectors that characterize the field in the medium: $\mathbf{E}$ is the electric field strength (V/m); $\mathbf{D}$ is the electric displacement (induction) (C/m^2); $\mathbf{H}$ is the magnetic field strength (A/m); $\mathbf{B}$ is the magnetic induction (T).

The four Maxwell's equations (10) are complemented by three equations that characterize the properties of the medium and establish the relationships between $\mathbf{D}$ and $\mathbf{E}$, $\mathbf{B}$ and $\mathbf{H}$, and $\mathbf{J}$ and $\mathbf{E}$:

$$\mathbf{J} = \sigma\mathbf{E},\ \mathbf{D} = \varepsilon\mathbf{E},\ \mathbf{B} = \mu\mathbf{H},$$

where σ is the specific electrical conductivity (S/m); $\varepsilon = \varepsilon_0\varepsilon_r$, $\varepsilon_0 = 8.85\times10^{-12}$ (F/m), ε_r is the relative permittivity of the medium; $\mu = \mu_0\mu_r$, $\mu_0 = 4\pi\times10^{-7}$(H/m), μ_r is the relative magnetic permeability of the medium.

Consider the simplest case where all characteristics of the media can be represented as constants, $\sigma = \text{const}$, $\varepsilon = \text{const}$, $\mu = \text{const}$.

To solve the problem for one of the fields (electric or magnetic), we transform to the second-order equations (Nechaev and Shurina, 2005).

Consider the transition to the second-order equation for the electric field vector $\mathbf{E}$:

$$\operatorname{rot}\mu^{-1}\operatorname{rot}\mathbf{E} = -(\partial/\partial t)\operatorname{rot}\mathbf{H}.$$

From the second equation of (10), $\operatorname{rot}\mathbf{H} = \varepsilon(\partial\mathbf{E}/\partial t) + \sigma\mathbf{E} + \mathbf{j}^{e}$, Consequently,

$$\operatorname{rot}\mu^{-1}\operatorname{rot}\mathbf{E} = -\varepsilon(\partial^2\mathbf{E}/\partial t^2) - \sigma(\partial\mathbf{E}/\partial t) - (\partial\mathbf{j}^{e}/\partial t). \tag{11}$$

In the modeling of the electric fields in the frequency domain, we assume that the components $\mathbf{j}^e$ and $\mathbf{E}$ of the resulting equation depend on time according to the harmonic law:

$$\mathbf{j}^{e} = \operatorname{Re}(\mathbf{j}^{e}_{r} + \mathbf{j}^{e}_{i})e^{i\omega t} = \mathbf{j}^{e}e^{i\omega t},\quad \mathbf{E} = \mathbf{E}e^{i\omega t} = (\mathbf{E}^{r} + i\mathbf{E}^{i})e^{i\omega t},$$

where i is the imaginary unit, $\omega = 2\pi f$ is the cyclic frequency, and f is the angular frequency.

The behavior of the electric field $\mathbf{E}$ harmonic in time is described by the vector Helmholtz equation:

$$\operatorname{rot}\mu^{-1}\operatorname{rot}\mathbf{E} - k^2\mathbf{E} = -i\omega\mathbf{j}^{e}, \tag{12}$$

where $k^2 = \omega^2\varepsilon - i\omega\sigma$ is the square of the wavenumber. For nonconducting media ($\sigma = 0$), this quantity is real, and in the quasi-stationary approximation, it is purely imaginary.

The simulation domain generally consists of subdomains with different electromagnetic properties. We consider the continuity conditions for the electric field $\mathbf{E}$ at the boundaries $\Gamma_{i,j}$ separating the subdomains with different physical properties. Then $\Omega = \cup_i \Omega_i$, where each of the domains Ω_i is characterized by its values of ε_i, μ_i, and σ_i. The continuity conditions of the electric field can be represented as

$$\left[\mathbf{n}\times\mathbf{E}\right]_{\Gamma} = 0,\ \left[\mathbf{n}\cdot(\sigma + i\omega\varepsilon)\mathbf{E}\right]_{\Gamma} = 0,$$

where $\mathbf{n}$ is the unit outer normal vector to the boundary.

Equation (12) should be complemented by boundary conditions in order for the problem of modeling the electric field to be well-posed. Consider a bounded open polyhedral region with Lipschitz continuous boundary $\partial\Omega$. Then the boundary conditions have the form $\mathbf{n}\times\mathbf{E}|_{\partial\Omega} = \mathbf{n}\times\mathbf{E}_0$. The homogeneous boundary conditions ($\mathbf{n}\times\mathbf{E}|_{\partial\Omega} = 0$) are specified on the boundaries of the region surrounded by a perfect conductor.

Tetrahedral finite elements are used because their geometric shape allows describing objects of high complexity (e.g., anticline trap). On the tetrahedral mesh cells, we define basis edge functions associated with the edges of the mesh of the finite-dimensional subspace $H^h(\text{rot};\Omega) \subset H(\text{rot};\Omega)$ (Nedelec, 1980). If $\sigma \neq \text{const}$ (seawater), the electrical conductivity function is involved in the construction of the basis edge functions, as described in more detail in (Marinenko et al., 2009).

Numerical experiments

We proceed directly to numerical calculations. The model characterizing each subdomain of the SEC is a parallelepiped with three subdomains corresponding to air, seawater, and the underlying medium (Fig. 3).

The SEC of the underlying medium is 0.1 S/m. The target object is an anticline trap buried to a depth of 50 m from the 330 m long interface between water and the underlying medium (Fig. 4).

Such a detailed description of the anticline trap model taking into account clay confining beds is due to the fact that, in our view, the latter can also indicate the presence of a petroleum reservoir. Due to the relatively low SEC, the latter may be poorly manifested in the measured signals and not always clearly differentiated from the signals arising from confining beds. The fact is that a clay confining bed has reduced SEC values. Moreover, the lower the permeability of the confining bed, the lower its CES. Sanding of a confining bed with an increase in its permeability leads to a reduction in the SEC values. Secondary pyritization of confining beds also indicates diffusion of volatile hydrocarbons and hydrogen sulfide into the rock overlying the trap. This is accompanied by electrical polarization processes described using the frequency dispersion (dependence) of the SEC and the appearance of its imaginary component. Thus, the target of marine geoelectrical exploration in searches for petroleum traps will be not only the traps, but also their overlying electrically conductive confining beds.

For water-saturated reservoirs, the SEC can vary (Epov et al., 2002) from 1/2 to 1/6 S/m, for oil-saturated reservoirs, from 1/4 to 1/50 S/m, for gas-saturated reservoirs, from 1/30 to 1/200 S/m, and finally for clay confining beds, from 1/2 to 1/6 S/m. In this study, we use the following values:

– water-saturated reservoir, 1/4 S/m at a depth of 50 m;
– oil-saturated reservoir, 1/40 S/m at a depth of 40 m;
– gas-saturated reservoir, 1/100 S/m at a depth of 30 m;

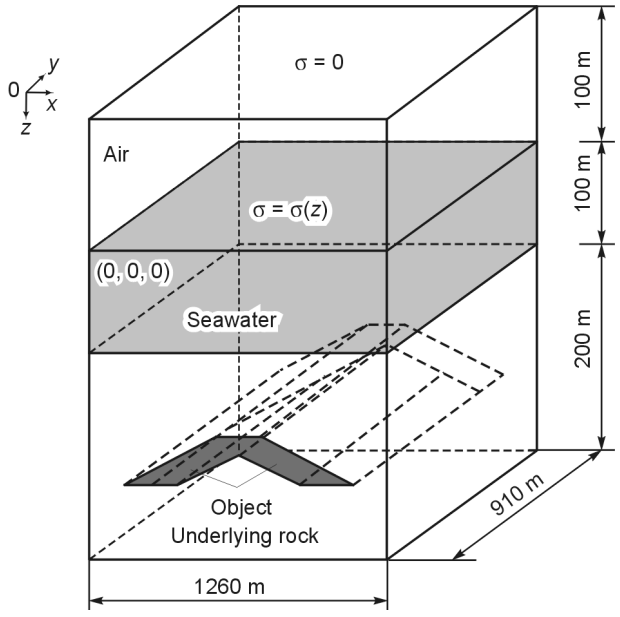

Fig. 3. Model of the environment and computation domain.

– clay beds—depending on the type of medium in contact with the bed—1/3 S/m for a bed in contact with gas, 1/3.5 S/m in contact with oil, and 1/4 S/m in contact with water.

The horizontal dimensions of reservoirs vary from 30 to 100 m (for a gas-saturated reservoir), and the thickness of the clay beds is about 20 m. In the constructed mathematical model, the shape and size of the reservoirs are identical on the left and right with respect the vertical axis passing through the top of the anticline trap (Fig. 4).

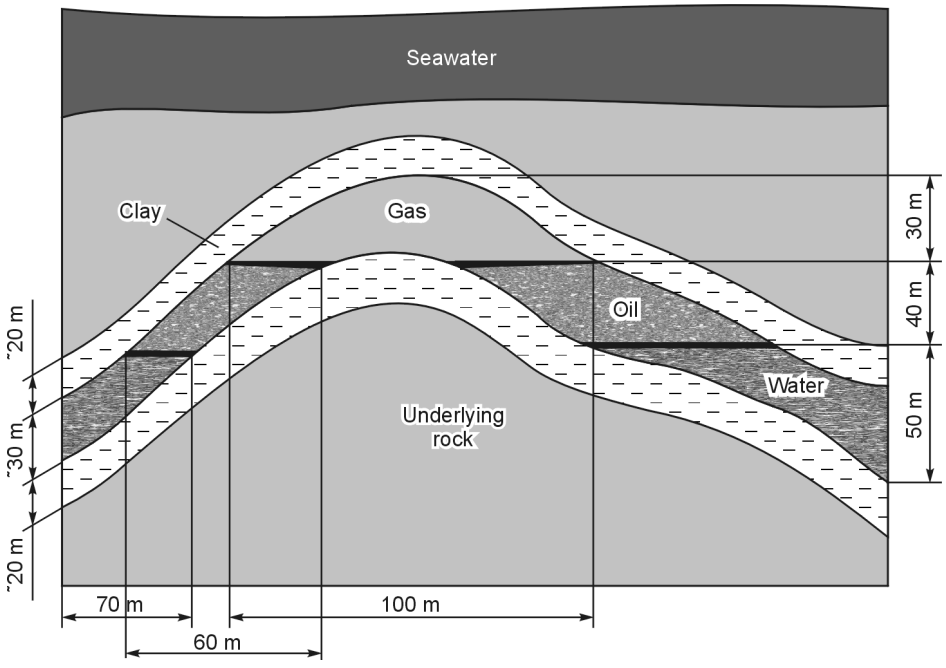

Fig. 4. Anticline trap model.

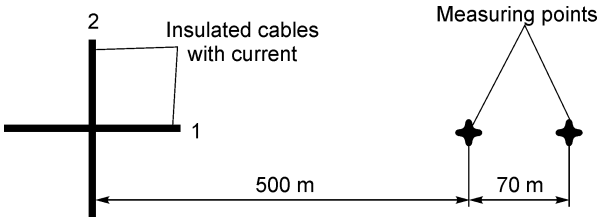

Fig. 5. Array model, top view.

The electrical conductivity distribution of seawater was varied depending on the task:

– a linear function (5 S/m near the water surface, and 7 S/m at the bottom)—a high gradient of 2 S/m;

– a linear function (5.5 S/m near the water surface, 6.5 S/m at the bottom)—a low gradient of 1 S/m;

– constant (6 S/m over the entire depth)—a gradient of 0 S/m.

Here the gradient is the difference between the SEC values near the bottom and the water surface.

The subsurface geoelectrical array, as mentioned earlier, consists of a pair of mutually perpendicular insulated cables of the same length (500 m) with two receivers arranged on one side of the source (Fig. 5).

Similar array parameters allow the use of the previously described approach to reduce the influence of the seawater layer in the model shown in Fig. 3.

Measurements are performed at nine positions of the array above the object (variable spacing).

The calculated phase difference between the contiguous measurement points is taken to be the measured parameter.

The aim of the first series of numerical experiments was to determine the frequency with the maximum sensitivity of the signal to the object. For this, we performed modeling starting at 3 Hz and doubling each next frequency. As a result, the effective frequency was determined to be equal to 12 Hz.

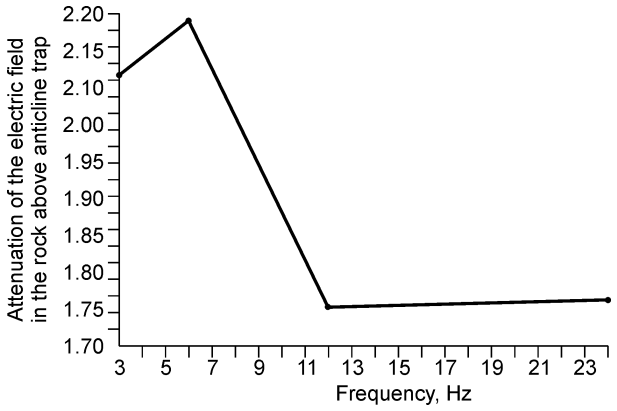

Fig. 6. Ratio of the amplitudes of the E_y component of the electric field on the surface and on the top of the anticlinal structure versus frequency.

To obtain the most accurate estimate of the depth of the method of investigation, the degree of attenuation of the electric field in the medium above the anticline trap is numerically calculated. Figure 6 shows the ratio of the electric-field amplitudes on the ground surface and on the top of the anticlinal structure versus frequency. Having determined the minimum attenuation of the signal in the frequency range, we obtain the frequency which may be called effective.

Using the value of effective frequency, we proceed to adjust the currents in the cables. The purpose of the adjustment is to increase the influence of the object on the measured signal so that its deviation from the signal in the medium without the object maximally exceeds the measurement error. The adjustment is made by changing the current in cable 2, while the current in cable 1 remains unchanged (100 A).

The adjustment of the current in the cables is carried out so that, in the reference model, the measured phase difference in the receiving electrodes was close to zero. The results of

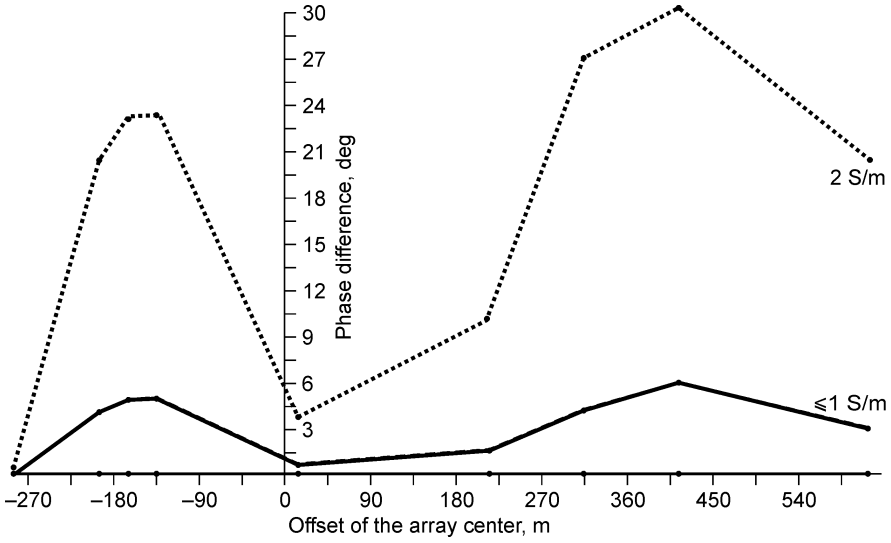

Fig. 7. Response to the object (phase difference) with a seawater electrical conductivity gradient.

the calculations show that the current in cable 2 depends on the vertical distribution of the seawater SEC:

– 224.3 A when the difference in SEC between the surface and depth is 2 S/m;

– 292.9 A when the difference in SEC between the surface and depth is 1 S/m;

– 359.8 A for constant SEC.

We proceed to the final step in the design aimed to maximize the response of the array to the object. The numerical modeling results are shown in Fig. 7.

Thus, it was possible to detect a response to the object equal to ~30° (difference of seawater SEC of 2 S/m) and 6° (difference of seawater SEC ≤1 S/m) (Fig. 7).

In the case of a small change in SEC, the effect of the additional space charge is not sufficient and the response to the object is no better than that in the case of constant SEC.

Conclusions

In this study, we were able to effectively combine an approach known in borehole geophysics with a new type of source, and the peculiar properties of seawater and obtained a result comparable with the best methods of surface electrical prospecting. This has made possible the revival of the near-surface marine geophysical methods which have been used at very shallow sea depths. We have shown that with a proper approach, subsurface geoelectric arrays are capable of conducting an efficient search for anticline traps located at depths of up to 150 m from the surface of water, and possibly deeper. In the proposed approach, however, there are some additional requirements for researchers and equipment. The first is the accuracy of setting the operating frequency, which is not a problem for modern devices and for numerical models. The second is the necessity of preliminary measurements in the working area, namely the determination of the depth of the seawater layer (to determine the dimensions of the array), the electrical-conductivity gradient of seawater, and the electrical conductivity of the underlying medium (to develop an accurate numerical model). It should be noted that preliminary measurements of varying accuracy and detail are performed in almost all geoelectric prospecting methods.

References

Connell, D., Key, K., 2013. A numerical comparison of time and frequency-domain marine electromagnetic methods for hydrocarbon exploration in shallow water. Geophysical Prospecting 61, 187–199.

Constable, S., Srnka, L.J., 2007. An introduction to marine controlled-source electromagnetic methods for hydrocarbon exploration. Geophysics 72 (2), WA3–WA12.

Davydycheva, S., Rykhlinski, N., 2011. Focused-source electromagnetic survey versus standard CSEM: 3D modeling in complex geometries. Geophysics 76 (1), F27–F41.

Epov, M.I., Antonov, Yu.N., 2000. VIKIZ Technology of Borehole Survey: Methodical Guide [in Russian]. OIGGM, Novosibirsk.

Epov, M.I., Antonov, Yu.N., Yeltsov, I.N., 2002. VIKIZ Method for Logging Oil and Gas Boreholes. Geo, Novosibirsk.

Jackson, J., 1962. Classical Electrodynamics. Wiley, New York,

Keithley Instruments, 2013. Low Level Measurements Handbook, 7th ed., URL: http://www.tek.com/keithley (access date 01.08.2016).

Landau, L.D., Lifshits, E.M., 2006. Theoretical Physics. Field Theory [in Russian]. Vol. 2, Fizmatlit, Moscow.

Louise, P., Gerald, W.H., 1995. A parametric study of the vertical electric source. Geophysics 60 (1), 43–52.

Luz, E.C., Regis, C.R.T., 2009. Influence of seawater resistivity on MCSEM data. Rev. Bras. Geof. 27 (3), 349–356.

Marinenko, A.V., Epov, M.I., Shurina, E.P., 2009. Properties of the electromagnetic field simulations in the coastal waters of seas. Russian Geology and Geophysics (Geologiya i Geofizika 50 (5), 475–484 (619–629).

Nechaev, O.V., Shurina, E.P., 2005. Multigrid algorithm for solving the three-dimensional Helmholtz equation using the vector finite element method. Matematicheskoe Modelirovanie 17 (6), 92–102.

Nedelec, J.C., 1980. Mixed finite elements in R^3. Number. Math. 35 (3), 315–341.

Rune, M., Tor, S.-P., 2007. Shaping optimal transmitter waveforms for marine CSEM surveys. SEG/San Antonio Annual Meeting, pp. 539–543.

Streich, R., Becken, M., 2011. Electromagnetic fields generated by finite-length wire sources: comparison with point dipole solutions. Geophysical Prospecting 59, 361–374.

Um, E.S., Alumbaugh, D.L., 2007. On the physics of the marine controlled-source electromagnetic method. Geophysics 72 (2), WA13–WA26.

Unesco, 1981. Background Papers and Supporting Data on the Practical Salinity Scale 1978. Unesco Technical Papers in Marine Science, No. 37, Paris.

Editorial responsibility: A.D. Duchkov